Results in Engineering 22 (2024) 102214

Contents lists available at ScienceDirect

Results in Engineering

journal homepage: www.sciencedirect.com/journal/results-in-engineering

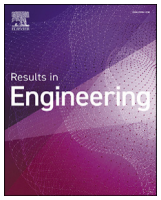

Research paper

Development of 6-way CFD-DEM-FEM momentum coupling interface using partitioned coupling approach

Prasad Adhav *, Xavier Besseron, Bernhard Peters

University of Luxembourg, Department of Engineering, Maison du Nombre, 6 Avenue de la Fonte, Esch-sur-Alzette, L-4364, Esch-sur-Alzette, Luxembourg

ARTICLE INFO

Keywords:
Multi-physics
Fluid-particle-structure interaction
Particle laden flow
Partitioned coupling
Volume coupling

ABSTRACT

Fluid-particle-structure interactions (FPSI) govern a wide range of natural and engineering phenomena, from landslides to erosion in abrasive water jet cutting nozzles. Despite the importance of studying FPSI, existing numerical frameworks often simplify or neglect certain physics, limiting their applicability. This work introduces a novel 6-way CFD-DEM-FEM momentum coupling for FPSI using a partitioned coupling approach, providing a flexible and adaptable solution.

Our prototype uses the preCICE coupling library to couple three numerical solvers: OpenFOAM for fluid dynamics, eXtended Discrete Element Method (XDEM) for particle motion, and CalculiX for structural mechanics. The coupling approach extends existing adapters and introduces a novel XDEM preCICE adapter, allowing data exchange over surface and volumetric meshes.

Numerical experiments successfully demonstrate the 6-way coupling, showcasing fluid-structure interactions and particle dynamics. The versatility of the partitioned coupling approach is highlighted, allowing the interchangeability of different single-physics solvers and facilitating the study of complex FPSI phenomena.

This article offers a thorough description of the methodology, coupling strategies, and detailed results, offering insights into the advantages and disadvantages of the proposed approach. This work lays the groundwork for a scalable and customizable FPSI simulation framework with a wide range of applications.

1. Introduction

Landslides, rock-ice avalanches, erosion and fracturing of oil pipes located underground or underwater, and leakage in sewer pipes all have a few things in common, the foremost important of them is disaster and damage caused leading to economic damages or even worse loss of human life. The other common factor among the listed is they are caused by the fluid-particle-structure interactions (FPSI). Apart from the phenomena described above, there are many more engineering fields requiring the study of FPSI.

The applications requiring these numerical methods can lead to great benefits, but very limited work has been done in the actual development of a coupled framework for FPSI. This is not due to the lack of motivation or resources but rather the sheer complexity involved in modeling. Many researchers have to weigh the cost of modeling such multi-scale, multi-physics phenomena partially or completely against the possible outcomes and the intended usage. Furthermore, the underlying multi-physical phenomena are complex and interact in a complex manner. Usually for the FPSI applications in consideration, the fluid and/or particle phase is the source of the momentum. These particle-laden flows then interact with a structure, that undergoes deformation due to exerted forces. This altered geometry of the structure in turn influences the flow characteristics. In some cases, such as the milling operation, the structure itself might be the source of momentum in the system.

A lot of work has been done over the years for modeling the fluid-structure interactions (FSI) using CFD-FEM [1] (Computational Fluid Dynamics - Finite Element Methods), furthermore using immersed boundary [2], and meshfree methods [3–5]. There is an extensive choice when it comes to FSI modeling, applied to applications such as aeroelasticity [6], biomedical applications involving blood flow [7], wind turbines [8], tidal turbines [9], bridge flutter [10], liquid filled pipes [11,12], etc.

Additionally, one can also find an abundance of particle-fluid interactions (PFI) [13,14]. Some of the applications include pneumatic conveyor [15], blast furnace simulations [16], granular flow [17], fluidised

* Corresponding author.
E-mail addresses: prasad.adhav@uni.lu (P. Adhav), xavier.besseron@uni.lu (X. Besseron), bernhard.peters@uni.lu (B. Peters).

https://doi.org/10.1016/j.rineng.2024.102214
Received 23 January 2024; Received in revised form 22 April 2024; Accepted 30 April 2024
Available online 7 May 2024

beds [18], rock ice avalanche [19], sand ejecting fire extinguisher [20], debris flow [21], pipe flow [22] etc.

In terms of particle-structure interaction (PSI), the popular applications are erosion [23], snow-tire interactions [24], abrasive water jet cutting [25], frictional behavior [26] etc.

Although the examples provided above for FSI, PFI, and PSI are not exhaustive, they show then extensive study and research done over the last years/decades, and the potential applications of such couplings. Some of the applications mentioned above are actually of FPSI, but one or more of the physics is not modeled for some or the other reason, thus leaving ample space for improvement. The examples provided above show that indeed a good foundation for FPSI exists, but very little work is done in this field.

Some noteworthy studies done in FPSI on the impact of debris flow on barriers/structures [27–29], usually applied for landslide/avalanches and their effects on man-made structures. These are very important phenomena to understand and study to implement better preventive structures against such disastrous forces. These works use Discrete Element Method (DEM) for the particle phase, Finite Element Method (FEM) for the structure, although they use different approaches for modeling the fluid. Smooth Particle Hydrodynamics (SPH) is used by [29] and [27]. On the contrary, [28] uses the Lattice Boltzmann Method (LBM) for modeling the fluid phase.

The FPSI is also used to study the pipe fracturing [30,31], where CFD, DEM, and/or FEM are used. In the literature, it is shown that it is important to study vibrations in pipes to better understand and prevent pipe wear, erosion, and fraction in [32,33]. Although, this research gap exists numerical FPSI framework has yet to be applied to such applications.

Additionally, FPSI is applied in modeling mills. SPH-DEM-FEM modeling is used by [34], whereas [35] uses coupling between particle finite element method (PFEM), DEM, and FEM. Apart from modeling the mill behavior, abrasive wear on the mill is also studied in [35].

Although sparse, the literature shows attempts at FPSI modeling. The literature presented above shows, that the fluid phase is mostly modeled using SPH, PFEM, or LBM. Although these might present advantages in terms of computational costs and free surface flows, they have limitations in terms of capturing certain physics, such as incompressibility or constant pressure boundaries. In the context of FPSI coupling using CFD, only two relevant studies, [30] and [36], are found in the literature. Furthermore, although the coupled environment might have all the components of FPSI, the coupling between these components might not be established, for example, [33] ignores the impacts of the particles on the structure, [30] uses 2-way coupling method between fluid-particle interaction, but used only 1-way coupling algorithm when considering interactions between structure and fluid-particles flow.

The different fields of engineering constantly face problems involving multi-scale, multi-physics and their complex interactions. Moreover, it is known from abundant literature that developing and working with coupled problems is challenging. This prohibits engineers, researchers, and scientists from completely realizing some problems and modeling certain multi-physics. In the FPSI literature presented above, generally, a monolithic coupling approach is utilized, with one exception [36]. In the FPSI by [36], the FSI part is implemented as a monolithic solver, whereas the interaction with particles is coupled using the partitioned approach. In a monolithic coupling approach, the different sets of segregated equations representing the different physics are solved iteratively. Such couplings are developed as a single code solver. For certain applications, the monolithic coupling approach may prove to be more robust. However, due to the nature of monolithic coupling, they are restricted to certain applications and offer little to no flexibility when modifying, extending, or adapting to new applications. Furthermore, increased fidelity in such multi-physics models implies increased requirement of computational resources, thus scaling for large, industrial, and high-fidelity applications can be a challenge [37–41].

In contrast to monolithic coupling, the partitioned approach couples high-level single-physics software currently available [39]. Utilizing this coupling approach allows the modification, exchange, add, or remove physics components from the multi-physics simulation environment, thus allowing us to address the growing complexity problem. The partitioned coupling approach also allows us to leverage the parallelization capabilities of the individual software involved efficiently and better load balancing required from different applications [41]. There are several open source coupling libraries/software to achieve such partitioned coupling approach, such as OpenPALM [42], Data Transfer Kit [43], Amuse [44], MuMMI [45], MUSCLE [46], MUI [47], preCICE [48] to name a few. From a review [49] on multi-scale coupling software, one can follow the logic to choose the correct coupling software. Hence, considering the possible applications, the availability of pre-existing single-physics software along with their ready-to-use adapters as the preCICE coupling library [48] is chosen to be used to establish the partitioned 6-way coupling between fluids, particles, and structures.

The preCICE coupling library allows us to circumvent the problems faced in monolithic coupling by treating the single-physics software/solvers as a black box. It enables communication, data mappings, time interpolations, and different coupling strategies thus providing much-needed flexibility when establishing a multi-scale, multi-physics simulation framework for FPSI. This further removes the need to have access or understanding to the solver source code, only the understanding of the usage and underlying physics is required. Additionally, due to the application programming interface (API) support for different languages such as C, C++, Python, MatLAB, Fortran, Julia, etc., solvers/software in different languages can be coupled.

The preCICE coupling library was developed originally to enable FSI [39], where the coupling is done over surface meshes. The preCICE coupling library and its adapters [50,51] have also been used to model Conjugate Heat transfer [52] between fluid and solids over surface meshes. Fracturing in poro-elastic medium due to fluid flow is simulated over volumetric meshes, but the coupled system uses surface terms for equilibrium. Although there are more multi-scale, multi-physics applications achieved using the preCICE coupling library, they are not relevant in the context of FPSI.

In the present work, a highly flexible, modifiable, and scalable partitioned coupling approach for fluid-particle-structure interaction (FPSI) through 6-way CFD-DEM-FEM momentum coupling is proposed. To the best knowledge of the authors, such a fully partitioned coupling approach has not yet been presented in the literature. As by the nature of the partitioned coupling approach, three different numerical solver/software are used, namely OpenFOAM [53] to simulate the fluids using CFD, eXtended Discrete Element Method (XDEM) [13] suite to solve for particle motion, and CalculiX [54,55] software is used to solve for structure deformations, stresses and vibrations. The fluid-structure and particle-structure interactions are achieved over surface meshes, whereas the fluid-particle Eulerian-Lagrangian interactions are achieved over volumetric meshes. The CFD is in the Eulerian framework, on the contrary, the DEM and FEM are in the Lagrangian framework. It should be noted that since the coupling is achieved over black box solvers/software, the single-physics software can be swapped, added, or removed altogether, as seen in Fig. 1.

To achieve the 6-way CFD-DEM-FEM partitioned momentum coupling, the pre-existing FSI coupling achieved over surface meshes is used, namely the OpenFOAM preCICE adapter [50], and CalculiX preCICE adapter [52,51]. Our contributions, which are novel or related to the 6-way partitioned momentum coupling for FPSI are, (1) developing an original XDEM preCICE adapter (the first DEM adapter developed) to enable data exchange over surface and volumetric meshes; (2) extending the OpenFOAM preCICE adapter to enable coupling over volumetric meshes; (3) presenting test cases to demonstrate 6-way momentum coupling, with using 2-way coupling as examples.

The article is arranged as follows: in section 2, the governing equations for each of the single-physics solvers involved are provided. Additionally, the mathematical model for accounting for coupled effects is also described. In section 3, the coupling strategies are explained more in detail along with a detailed description of the XDEM pre-CICE adapter. In section 4, the results demonstrating the coupled FPSI behavior are presented. Additionally, FPSI numerical experiments are compared to the FPSI experimental observations. In section 5, the results, their impacts, and insights are discussed along with the strengths and weaknesses of the proposed coupling approach. Future work and possibilities for applying the 6-way coupling are also explored. Finally, in the section 6, the concluding remarks are presented.

2. Model description

In the partitioned coupling approach, three different software are used to establish a multi-physics environment to couple momentum between fluids, particles, and structures. These physics are simulated using CFD, DEM, and FEM respectively. The governing equations of the respective numerical methods are described below.

2.1. Governing equations for discrete particles

XDEM software suite [13] is used in the current work to model the discrete particle phase. XDEM models both dynamics as well as thermodynamics of the particulate system. In the current work, the main focus will be the dynamic behavior of particles interacting with fluids and structures. The particle position, velocity, and acceleration are computed with the dynamics module of the XDEM.

The discrete element method (DEM) used in the dynamics module of XDEM is based on the soft sphere model. In this method, it is assumed that the particles are deformable and can overlap each other, where the magnitude of overlap is decided by the contact force using the force-displacement law. The hardness of the particle is expressed via Young's Modulus, while the particle energy dissipation is described with a dampener and/or dashpot. The translational and rotational movements of individual particles are tracked using classical mechanics equations. A detailed description of all the terms mentioned below can be found in previous work [56]. A summary of the translational and rotational motion equations is given below: Equations of particle motion:

$$m_i \frac{d\vec{v}_i}{dt} = m_i \frac{d^2\vec{X}_i}{dt^2} = \vec{F}_i^c + \vec{F}_i^g + \vec{F}_i^{ext} \tag{2.1}$$

where $\vec{X}_i$ is the position vector for a given particle, and $\vec{u}_{p_i}$ is particle velocity. $\vec{F}_i^g$ is the force due to gravity. $\vec{F}_i^{ext}$ is the sum of all the external forces acting on the particle, such as (hydrostatic) buoyancy forces $\vec{F}_B$ and (hydrodynamic) drag forces $\vec{F}_D$. $\vec{F}_i^c$ is the force due to the collision of particles, which is discussed further in equation (2.6).

$$I_i \frac{d\vec{\phi}_i}{dt} = \vec{M}_c + \vec{M}_{ext} + \vec{M}_{roll} \tag{2.2}$$

where I_i is the moment of inertia, $\vec{\phi}_i$ is the orientation, $\vec{M}_c$ stands for the torque acting due to inter-particle collisions, $\vec{M}_{ext}$ is the torque acting on the particles from external sources. The $\vec{M}_{roll}$ is the torque acting due to rolling friction given as follows:

$$\vec{M}_{roll} = -\mu_r |\vec{F}_n| R_i \frac{\vec{\omega}}{|\omega|} \tag{2.3}$$

where $\vec{F}_n$ is the normal force derived from the Hertz theory [57] for the normal elastic force whereas Mindlin's work [58] is used to compute the normal energy dissipation, given as follows:

$$\vec{F}_n = -\left(\frac{4}{3} E_{ij} \sqrt{R_{ij}} \delta^{\frac{3}{2}} + c_n \delta^{\frac{1}{4}} \dot{\delta}\right) \tag{2.4}$$

where c_n is the normal dissipation coefficient proposed by Tsuji et al. E_{ij} is the effective Young's modulus, R_{ij} is the reduced radius, δ is the overlap between the particles. The normal dissipation coefficient is expressed as proposed by Tsuji et al. [59] and Zhang and Whitten [60]. The tangential forces include static and dynamic friction as follows:

$$\vec{F}_t = \min\left(k_t \delta_t + c_t \dot{\delta}_t, \mu \vec{F}_n\right) \tag{2.5}$$

where, k_t is tangential stiffness, c_t is tangential dissipation coefficient, δ_t is the tangential displacement or tangential slip, μ is the friction coefficient, and $\vec{F}_n$ is described in equation (2.4).
The inter-particle collision forces and torques are given as follows:

$$\vec{F}_i^c = \sum_{i \neq j} \vec{F}_{i,j}(\vec{X}_j, \vec{u}_{p_j}, \vec{\phi}_j, \vec{\omega}_j) \tag{2.6}$$

$$\vec{M}_i^c = \sum_{i \neq j} \vec{M}_{i,j}(\vec{X}_j, \vec{u}_{p_j}, \vec{\phi}_j, \vec{\omega}_j) \tag{2.7}$$

where the for $\vec{F}_i^c$ stands for the collision forces between the particles, $\vec{M}_i^c$ is the torque due to collisions, $\vec{F}_{i,j}$ and $\vec{M}_{i,j}$ is the force and torque exerted by particle j on particle i respectively, $\vec{\omega}$ is the particle angular velocity. The sum $\sum_{i \neq j}$ represents the sum over all particles other than i.

Two colliding bodies will deform at the contact, and causing stresses at the contact surfaces [61]. However, when considering the particulate system, the stresses at the contact are generally of no interest. Hence, in DEM [62], the particle-to-particle collisions and the results forces are computed based on the overlap. This overlap method is commonly used as it is a physically intuitive, and straightforward way to determine interaction between two particles. Similarly, the collisions between particles and walls are resolved with the overlap method, where the collision forces are computed based on the overlap between the particle and the wall. Hence, it should be noted that any boundaries, walls, or drums in the current work are treated as another particle, to compute the above-mentioned collision forces between particles and walls. This allows tracking the interactions between particles and walls, without requiring to solve for stresses on the wall. Furthermore, the collision forces are available on the wall, at the location of particle impacts. Therefore, the collisions with boundaries/walls/drum are considered in the equations (2.6) and (2.7). In the equation (2.1), the term $\vec{F}_i^{ext}$ accounts for the fluid forces acting on the particle discussed further in section 2.4.1.

2.2. Governing equations for fluid

In the Eulerian volumetric average method, the conservation equation of mass (Eq (2.8)) and momentum (Eq (2.9)) are written over a representative volume. Conservation of mass

$$\frac{\partial}{\partial t}\left(\rho_f\right) + \nabla \cdot \left(\rho_f \vec{u}_f\right) = m' \tag{2.8}$$

Conservation of momentum

$$\frac{\partial}{\partial t}\left(\rho_f \vec{u}_f\right) + \nabla \cdot \left(\rho_f \vec{u}_f \vec{u}_f\right) = -\nabla p + \rho_f \vec{g} + \mu_f \nabla^2 \vec{u}_f + \vec{S} \tag{2.9}$$

2.3. Governing equations for solid structures

The structures in the current work are modeled using the Finite Element Method (FEM). In this method, a large continuous problem (continuum) is discretized into smaller and simpler "finite elements". In this manner the underlying partial differential equations (PDEs) do not need to be solved over the complete spatial domain, but rather over a small element [63]. It is to be noted that FEM is a method to solve a set of PDEs, hence, depending on the underlying governing equations different physics can be modeled. In the current work, the displacements and the stresses of the structures are of interest.

The governing equations for displacements and stresses in a structure are derived from the principles of continuum mechanics and material behavior under consideration. The equilibrium equations express the balance of forces within the structure. They are derived from the principle of virtual work and are used to establish the equilibrium of internal and external forces. In matrix form, the equilibrium equations can be expressed as:

$$\mathbf{K} \cdot \vec{U} = -\vec{f} \tag{2.10}$$

where $\mathbf{K}$ is the global stiffness matrix, $\vec{U}$ is the vector of nodal displacements and $\vec{f}$ is the vector of applied nodal forces.

The constitutive equations relate stresses to strains for the material being analyzed. For linear elastic materials, Hooke's law is commonly used to express the relationship between stress and strain:

$$\boldsymbol{\sigma} = \mathbf{D} \cdot \boldsymbol{\epsilon} \tag{2.11}$$

where $\boldsymbol{\sigma}$ is the stress tensor, $\mathbf{D}$ is the elasticity matrix and $\boldsymbol{\epsilon}$ is the strain tensor.

The relationship between strains and displacements is defined based on the assumed displacement field within each finite element. This relationship is typically expressed using the strain-displacement matrix, which relates the strains to the nodal displacements within an element.

$$\boldsymbol{\epsilon} = \mathbf{B} \cdot \vec{U} \tag{2.12}$$

where $\mathbf{B}$ is the strain-displacement matrix, that is dependent on the type of elements, and shape function used.

By combining the equilibrium equations, constitutive equations, and the strain-displacement relationship, a system of equations can be formulated to solve for the nodal displacements and subsequently calculate the stresses within the structure.

In the current work, Calculix [54,55] an open-source, three-dimensional FEM software is used to solve the structure displacements and stresses on unstructured Lagrangian meshes. The readers are referred to the standard textbooks on FEM [63–66] for further reading.

2.4. CFD-DEM coupling

The CFD-DEM Eulerian-Lagrangian coupling is achieved over a volumetric mesh. In this section, the equations utilized to represent the coupled physics are presented. This work deals with single-phase as well as multi-phase fluids. Consequently, the equations presented in the following subsections, consider these different fluid conditions.

2.4.1. Fluid forces acting on particles

In this section, the effects of fluid forces acting on the particles are formulated. The DEM solver receives the fluid fields and properties and uses the following equations to compute the fluid forces acting on the particles. There are two types of fluid forces acting on the particles, namely hydrostatic or pressure force, and hydrodynamic or momentum exchange force. The hydrostatic force is the buoyancy force that accounts for the pressure gradient around an individual particle [67].

$$\vec{F}_B = -V_{p_i} \boldsymbol{\nabla} p \tag{2.13}$$

where $\vec{F}_B$ is the buoyancy force, V_{p_i} is the volume of particle under consideration and $\boldsymbol{\nabla} p$ is the gradient of pressure experienced by the particle.

To compute the momentum exchange or hydrodynamics forces acting on the particles, first, the porosity i.e. the space fraction occupied by particles is computed. The porosity/void fraction of particles in fluid is given as:

$$\epsilon = 1 - \frac{1}{V_c} \sum_{i}^{n} \eta_i V_{p_i} \tag{2.14}$$

where V_c is the cell volume containing the particle, V_{p_i} is the volume of the i^{th} particle in the cell, and *eta* is the weight used for the porosity computation depending on the particle volume present inside the current cell.

In the Eulerian-Lagrangian approach, the hydrodynamic force corresponds to the fluid-particle interaction. This force depends on the relative velocity of the solid particle and fluid along with the forces acting due to the presence of neighboring particles. The drag force acting on the particle can be expressed as the relative velocity mentioned above and a momentum transfer coefficient β, described as the default drag model given by Shiller-Neumann [68]. Shiller-Neumann [68] is best suited when predicting drag for non-spherical particles. The correlations of β are obtained from pressure drop measurements for fixed, fluidized, or settling beds [69]. Several drag laws are implemented in the XDEM suite.

A drag model proposed by Richardson-Zaki [70] considers an exponent dependent on the Reynolds number based on the particle terminal velocity. Richardson-Zaki [70] is suitable for simulations focusing on bed expansion and packing, often applied in fluidized bed reactors and granular flow studies.

Gidaspow [71] combines Ergun and Orning [72], and Wen and Yu [73] for sense and dilute phase calculations respectively, along with a switch function to transition from one regime to the other. Gidaspow [71] is suitable for a broad range of particulate systems, including applications in chemical engineering and fluidized bed reactors.

di Felice [74] gave a new transition function based on the particle Reynolds number. di Felice [74] is useful for simulations where the kinetic behavior of particles, especially collisions, and energy dissipation, is crucial, such as in pneumatic conveying or slurry flows.

Syamal-OBrien [75] uses particle terminal velocities in fluidized or settling beds to formulate β. Syamal-OBrien [75] is ideal for simulations involving a large number of particles, such as in industrial-scale fluidized bed reactors.

Sun-Battagli [76] proposed a model specifically designed for porous beds using CFD-DEM solutions. Sun-Battagli [76] is useful for simulations involving particle clustering, such as in fluidized beds with agglomerating particles.

Finally, Arastoopour [77] gave a model for β that is continuous over all values of void fraction (ϵ).

In the current work, the particle flow is varied, occurring in both sparse and densely packed arrangements. According to studies [69], Gidaspow [71] model gave the best agreement with the experimental observations both qualitatively and quantitatively [69]. The drag force acting on the particle due to the fluid for the CFD-DEM approach used in the current study is given as follows:

$$\vec{F}_D = \frac{\beta V_p}{(1-\epsilon)} \left(\vec{u}_f - \vec{u}_p \right) \tag{2.15}$$

The interphase momentum exchange β is predicted according to Gidaspow [71]. Although to cover all range of void fraction (ϵ), Wen and Yu [73] ($\epsilon \geq 0.8$) and Ergun and Orning [72] ($\epsilon < 0.8$) equations are included. Combining these equations allows capturing drag calculations for densely packed and sparsely packed particles.

$$\beta = \begin{cases} 150 \dfrac{(1-\epsilon)^2}{\epsilon} \dfrac{\mu_f}{d_p^2} + 1.75(1-\epsilon) \dfrac{\rho_f}{d_p} |\vec{u}_f - \vec{u}_p|, & \text{if} \quad \epsilon < 0.8 \\ \dfrac{3}{2} C_d \dfrac{\epsilon(1-\epsilon)^2}{d_p} \rho_f |\vec{u}_f - \vec{u}_p| \epsilon^{-2.65}, & \text{if} \quad \epsilon \geq 0.8 \end{cases} \tag{2.16}$$

where the drag coefficient C_d is given as:

$$C_d = \begin{cases} \dfrac{24}{Re} \left[1 + 0.15 (Re)^{0.687} \right], & \text{if} \quad \text{Re} < 1000 \\ 0.44, & \text{if} \quad \text{Re} \geq 1000 \end{cases} \tag{2.17}$$

and the Reynolds number for the particle is given as:

$$Re = \frac{\epsilon \rho_f |\vec{u}_f - \vec{u}_p| d_p}{\mu_f} \tag{2.18}$$

2.4.2. Particle momentum source terms

Due to the nature of the momentum coupling under consideration, there are different possibilities for momentum exchange between fluids and particles as follows: the fluid can be the driving force, imparting momentum on the particles, consequently the particles offer resistance (drag source) to the fluid motion; the particles can be the source of momentum, imparting motion on the fluid by exerting acceleration on it; or lastly due to the complex nature of the application both conditions stated above can take place simultaneously in the different parts of the simulation domain. Therefore the momentum exerted by the solid particles on the fluid is treated in a semi-implicit way according to the method proposed by Xiao and Sun [78]. The explicit momentum source term $\vec{A}_c$ and implicit momentum source term Ω_c are as given in Eq (2.19)

$$\vec{A}_c = \frac{1}{\rho_f V_c} \widetilde{\sum_i} B_i \vec{u}_{p_i}, \quad \Omega_c = \frac{1}{\rho_f V_c} \sum_{i=1}^{c_n} B_i \tag{2.19}$$

where the coefficient B_i [78] depends on the particle velocity $\vec{u}_p$, fluid velocity for the cell containing the particle $\vec{u_{f_c}}$, drag coefficient C_d and particle diameter d_p. Thus giving the source term to be injected in equation (2.9) as follows:

$$\vec{S} = \rho_f \vec{A}_c - \rho_f \Omega_c \vec{u}_{f_c} \tag{2.20}$$

Alternatively, if the application demands it, the particles can be represented in the fluid phase only as a drag source term S_i. The drag source is computed based on the Darcy–Forchheimer law [79,80] for porous media, which is comprised of a viscous loss term and an inertial loss term. This creates a pressure drop proportional to the fluid velocity and velocity squared, respectively.

$$\vec{S} = -\left(\mu_f D + \frac{1}{2}\rho \vec{u_f} F\right) \vec{u_f} \tag{2.21}$$

where D and F are Darcy–Forchheimer coefficients computed as follows:

$$\begin{aligned} D &= \frac{d_p^2}{150} \frac{\epsilon^3}{(1-\epsilon)^2} \\ F &= \frac{d_p}{3.5} \frac{\epsilon^3}{(1-\epsilon)} \end{aligned} \tag{2.22}$$

where d_p is the mean particle diameter assuming that the porous media is comprised of spherical particles, and ϵ is the volume porosity defined in equation (2.14).

2.5. CFD-FEM and DEM-FEM coupling

The CFD-FEM and DEM-FEM coupling is achieved over a surface mesh. The structure is usually a moving boundary patch in the CFD domain. The pressure field of the fluid acting over the structure surface is used to compute the forces exerted by fluid, thus computing pressure over the CFD cell face area. These forces are communicated over to the nodes of the structure.

The DEM solver uses STL to represent the structure in the DEM simulation domain. This STL wall is treated as just another particle, and thus it is possible to capture the inter-particle interactions. However in this case the particle forces acting on the triangles of the STL file are captured. The forces are then distributed over the three points of the triangles. These forces on the STL "nodes" are then communicated to the FEM solver.

The FEM solver receives fluid/particle forces as an input. These forces are then summed up. The forces are then applied as Neumann boundary conditions.

Neumann boundary conditions specify the applied forces or traction on the boundaries of the domain [63], given as follows:

$$t_i = t_{i,0} \quad \text{for } i \in \Gamma_t \tag{2.23}$$

where t_i is the traction on the i^{th} degree of freedom, $t_{i,0}$ is the prescribed value of traction and Γ_t is the set of degrees of freedom on which the Neumann boundary conditions are applied.

Once the FEM solver receives the forces exerted by the CFD/DEM solver, and they are applied as Neumann boundary condition using the `*CLOAD` card in CalculiX, the FEM solver then solves for the displacements in the structure. These displacements are then communicated to the CFD and the DEM solvers.

The CFD solver represents the structure as a moving wall, hence the CFD mesh is moved according to the displacements. On the contrary, as DEM is a meshless method, and the structure is represented as an STL wall, the displacements are directly applied to the STL wall and it is deformed. This is equivalent to changing the shape of a particle.

3. Coupling approach

The preCICE coupling library uses high-level APIs to minimize the invasion in the solver code base by using adapters. In the context of the current work an "adapter" is what is referred to as this preCICE integration into the solver [51]. Furthermore, an API for a well-developed solver, be it open-source, internally developed, or otherwise, is typically available. On the contrary, if one wishes to couple an in-house solver, due to indigenous development, the code base is well understood and ad-hoc API can be implemented. The adapter can be easily implemented and compiled as a separate library that the solver calls during runtime by using the API from the solver and preCICE, which keeps the solver code intact. In a coupled simulation, the adapter receives the necessary data from the solver and relays it to the other coupled solver(s) via preCICE (MPI ports or TCP/IP sockets). An outline for the partitioned coupling is presented in Fig. 1.

3.1. OpenFOAM adapter for preCICE coupling

The preCICE coupling library provides an OpenFOAM adapter [50] that can handle surface coupling preliminarily used for Fluid-Structure interaction (FSI) and Conjugate Heat Transfer (CHT). The adapter out of the box is not equipped to handle volume coupling but rather extended by the users [50]. The OpenFOAM adapter does not have all the fields required for the CFD-DEM volume coupling intended for momentum exchange, some that are available, are defined over the surface mesh. Hence, it was necessary to implement and develop this part for the adapter.

To enable the volume coupling, a new coupling interface is implemented in the OpenFOAM adapter consisting of two modules, namely, Fluid Properties and Momentum Transfer. A simplified class UML diagram is presented in the Fig. 2, illustrating the new additions and modifications in the OpenFOAM adapter (represented using a solid outline, whereas the dashed outline is a pre-existing implementation). The muted colors represent pre-existing classes, whereas the bright colors show the modifications added to the current work.

As described in section 2.4.1, fluid fields such as fluid velocity, density, viscosity, pressure gradient, and phase volume fraction gradient are required for computing the fluid forces/effects on the particles. Hence, these fields are implemented in the Fluid Properties module, as they are not tied to CFD-DEM coupling per-say rather they are the data fields available for volume coupling representing the fluid state. As the class structure exists, one may add further fluid fields. The data fields coming from the DEM are added to the Momentum Transfer module. These fields represent the particle momentum contribution in the fluid phase as described in section 2.4.2. They consist of volume porosity, acceleration, omega, and particle diameter. Depending on the type of flow, different particle representation is used. For example, packed beds offer only drag (or pressure drop) to the fluid. Hence, in such cases, the volume porosity can be used to compute the drag based on

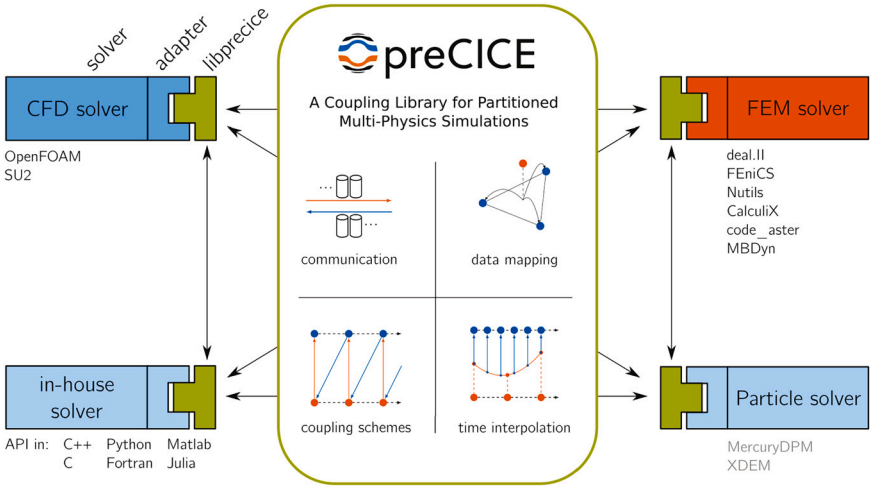

Fig. 1. A schematic outlining the coupling procedure [81] (reproduced with permission).

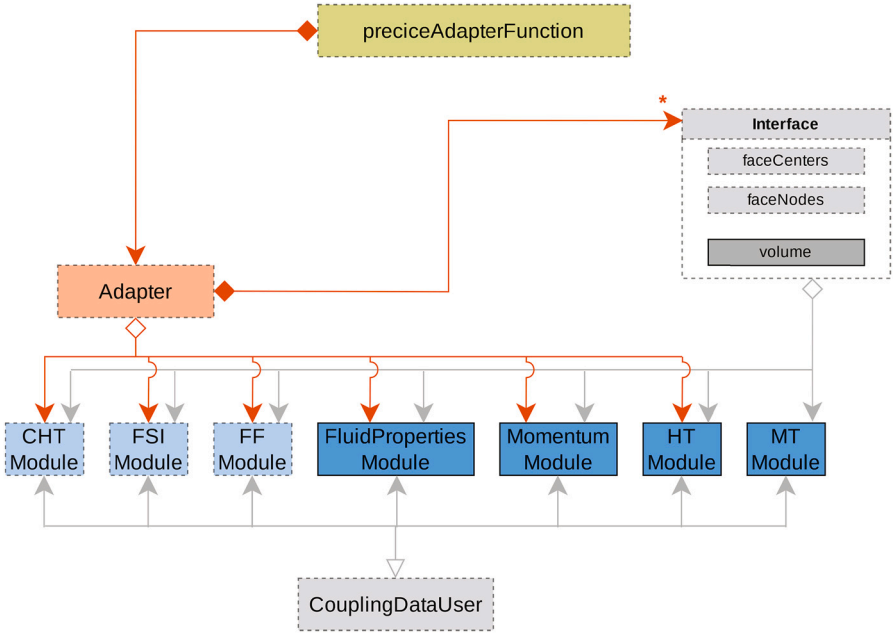

Fig. 2. A simplified class UML diagram for the modified OpenFOAM adapter.

Darcy–Forchheimer law. On the contrary, moving particles may offer drag or acceleration to the fluid, in such case, acceleration and omega, semi-implicit momentum source term is used.

Irrespective of the drag representation used, the drag is injected or represented in the fluid phase using the `fvOptions` dictionary (renamed as `fvModels` since OpenFOAM v9). Hence, there is no need for any invasive modifications in the CFD solver code base. In a broader scope, OpenFOAM provides various solvers representing different flow conditions and utilizes different algorithms for solving the governing equations. Irrespective of the solver used, the same fields can be used for representing the particles in the fluid phase.

3.2. XDEM adapter for preCICE coupling

The XDEM software suite is implemented in C++, thus when the XDEM preCICE adapter is also implemented in C++. The C++ API of preCICE is used to call and utilize the coupling library. It is to be noted that such API is also provided in various programming languages such as C, MatLAB, Python, Fortran, Julia, etc. Thus, when implementing an adapter for an in-house solver written in the above-mentioned programming languages is straightforward using the API for the respective language.

The XDEM adapter is implemented to be flexible for diverse types of applications, following the guidelines from the preCICE coupling library. A simplified class UML diagram for the XDEM adapter is presented in Fig. 3, illustrating the adapter structure. The XDEM software suite consists of several solvers, purpose-built for certain applications. The `xdem-adapter` thus is compiled just as another XDEM solver. The XDEM solvers usually expect one argument, i.e. the input file name, but in the case of the XDEM preCICE adapter, it also needs the name of the preCICE configuration file as an argument. As the adapter handles all the simulation types, it checks which simulation types are needed using the preCICE configuration and XDEM input file. Depending on this it will create `Coupled_Object` for each of the coupling done. The XDEM preCICE adapter allows the selection and use of any data fields. Additionally, if a field is required but not exchanged it will set default values for that field, implemented in the `Deformable_object_Implementation` and `Fluid_object_Implementation`. The XDEM adapter also provides a summary of the exchanged data fields and the possible type of simulation being run based on the data fields used.

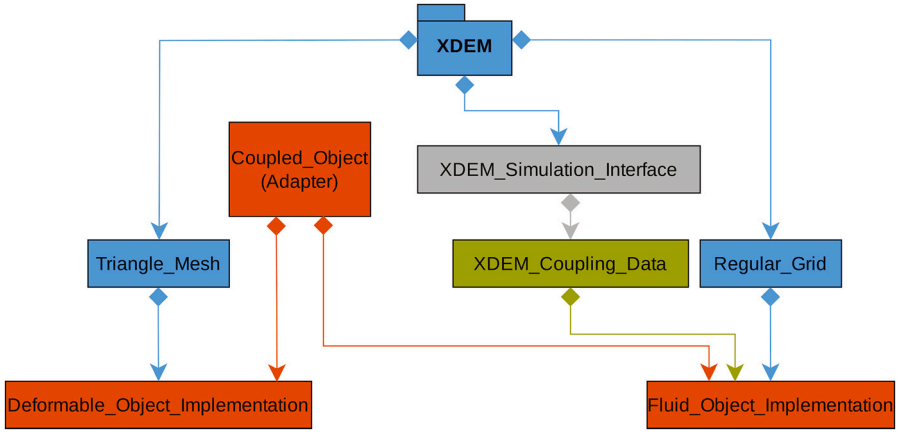

Fig. 3. A simplified class UML diagram for the XDEM adapter.

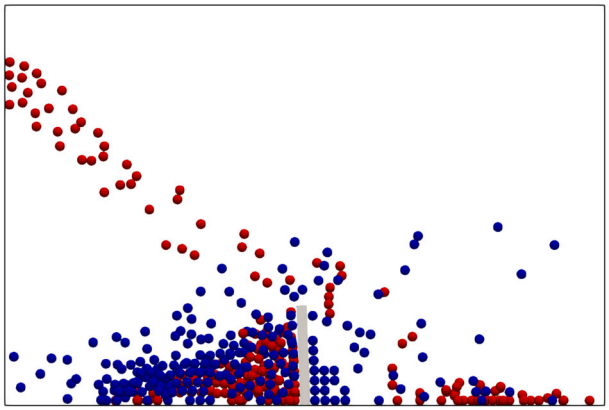

Fig. 4. DEM simulation domain displaying the particle positions of heavy (red) and light (blue) particles.

The XDEM adapter receives several fluid fields describing the flow conditions. Based on these fields the fluid forces (drag) on the particles are computed and applied as external forces. Several drag laws are available in XDEM, as described in section 2.4.1, that utilize the fluid fields to compute the fluid drag acting on the particles.

Additionally, using the particle state, either the volume porosity or the seim-implicit momentum source is computed and transferred by XDEM through the XDEM adapter. This reduces the computation cost of the fluid solver.

3.3. Volume coupling

The XDEM software suite is based on the discrete element method, which is a meshless method. This poses the largest challenge when coupling such meshless methods with mesh-based methods. In the current work, although the DEM solver is a meshless method, due to the computational costs a lot of work has been done to parallelize the solver and improve performance [40,37,82,41,83]. Due to the requirement of parallelization, the meshless domain is divided into several small parts thus providing a pseudo mesh/structure. For the volume coupling, this pseudo mesh is used to exchange the coupling data.

In Fig. 4, a side view of the flow through channel case is presented in section 4.2. More details on the simulation set are available in the mentioned section, as the current section focuses on the volume coupling itself. The XDEM simulation domain is initially just a box, where the particle position is tracked, if the particle leaves this spatial domain it is deleted from the simulation. The Fig. 5 (a), shows this XDEM simulation domain is discretized, with the crosses showing the centers of the volumes. The Fig. 5 (b) shows the meshed fluid domain. As the CFD uses finite volume methods, the mesh volumes and cell centers are already available and represented here as squares.

These volume/cell centers are used to exchange the coupling data. As it can be seen in Fig. 5 the DEM and the CFD mesh do not entirely conform. This is because in the DEM domain, the structure is treated just like another particle, but with some additional properties, represented with a STL file. On the contrary, in the CFD, only the fluid domain is present, while the space for the structural domain is left out. Even though the CFD and DEM domains have non-conforming meshes, it is not an issue due to the data mapping schemes available. These data mapping schemes will interpolate the data between the cell centers that do conform.

In the Fig. 5, an example of scalar data mapping is shown from DEM to the CFD domain. The particles may be represented in the fluid domain as a drag source using porosity. The same is seen in Fig. 5, where Volume porosity represents the particles. XDEM computes this volume porosity, a scalar, and stores these values at the cell centers. When comparing the particle positions shown in Fig. 4 and the volume porosity shown in Fig. 5 (a), it can be seen that it represents the particle positions well. The XDEM grid can be refined further to capture the variables better, in this case, the volume porosity. Nonetheless, the data mapping strategies allow for mapping the data well. Due to the nature of the volume coupling used along with the data mapping, this type of volume coupling offers flexibility in choosing the CFD mesh size and the particle size used in the unresolved CFD-DEM coupling.

Fig. 5 (b), illustrates the volume porosity after it is mapped onto the CFD mesh. The Fig. 5 (a) and (b) only show the volume porosity values at the volume/cell centers. To further illustrate the data mapping, a slice of the fluid domain with the XDEM cell centers and volume porosity is shown in Fig. 6. Similarly, all the other fields are transferred and mapped using these volume/cell centers in both directions of the coupling. Additionally, if the CFD data is made available on the CFD volume centers, then theoretically any given CFD software tool/package can be used to achieve this CFD-DEM partitioned volume coupling.

3.4. Surface coupling

The CFD-FEM surface coupling used in the current study is standard out of the box. It is well described and validated in the literature [84, 50] using the Turek-Horn FSI2 and FSI3 benchmarks [85]. Thus the surface coupling between fluid and structure is not discussed further in the current work.

The surface coupling did not exist between the DEM and the FEM solver. However, the FEM preCICE adapter is used out of the box for this coupling. The FEM solver is not specified in this case as any FEM solver with the preCICE adapters can be used as the fields required for such coupling are common among the existing FEM preCICE adapters, namely forces and displacements.

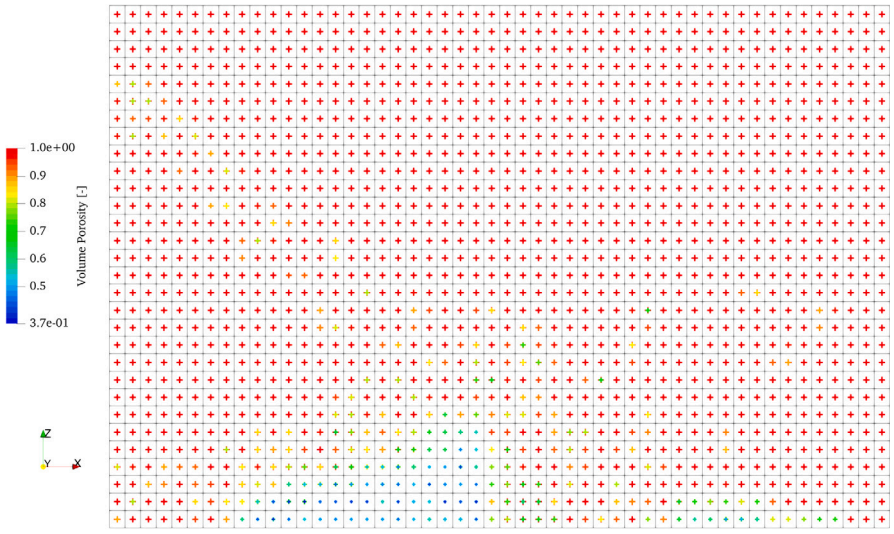

(a) XDEM discretized domain

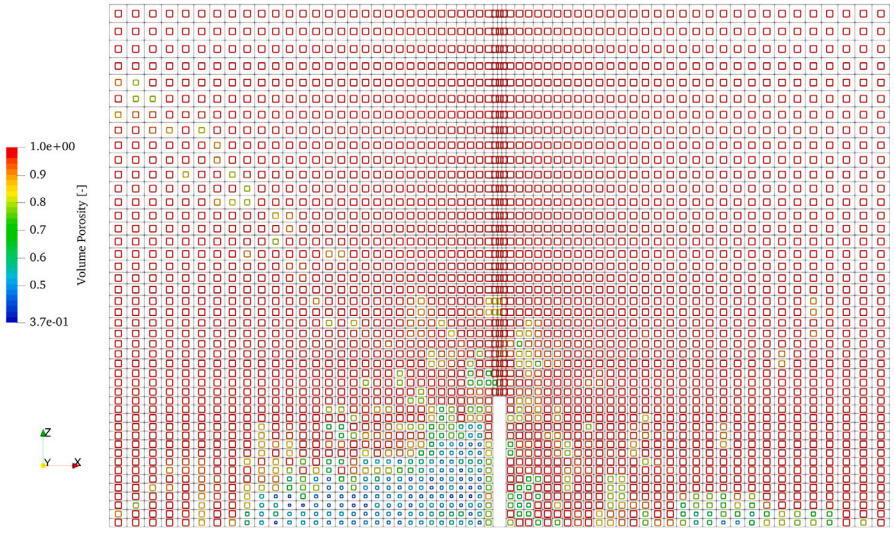

(b) Fluid Mesh

Fig. 5. DEM and fluid domain with their volume and cell centers respectively, colored and scaled using the volume porosity.

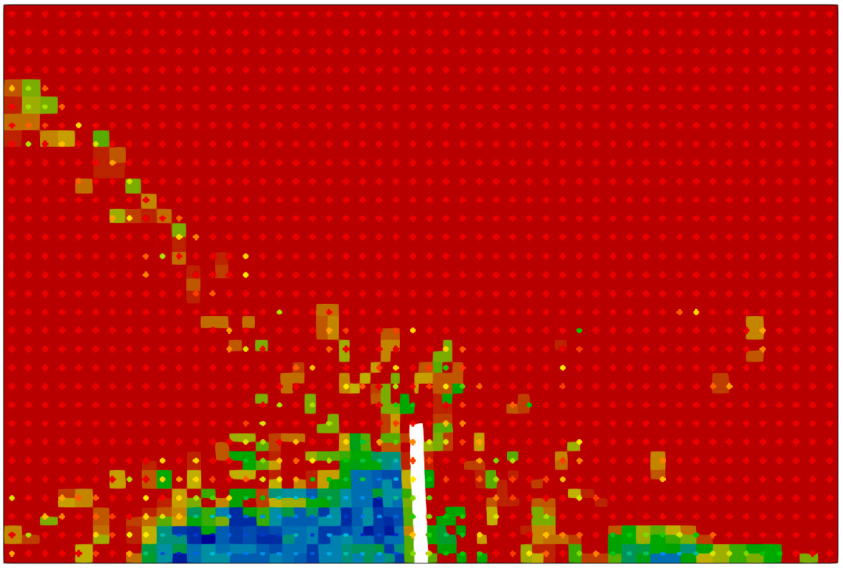

Fig. 6. Fluid slice showing volume porosity field with the XDEM cell centers.

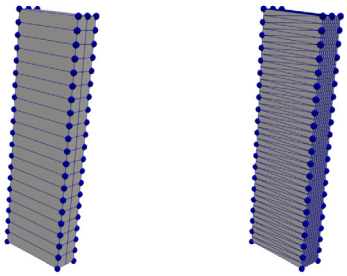

(a) FEM mesh with nodes (b) XDEM STL wall with nodes

Fig. 7. FEM and XDEM mesh with the nodes used to exchange data with one cell in z-direction.

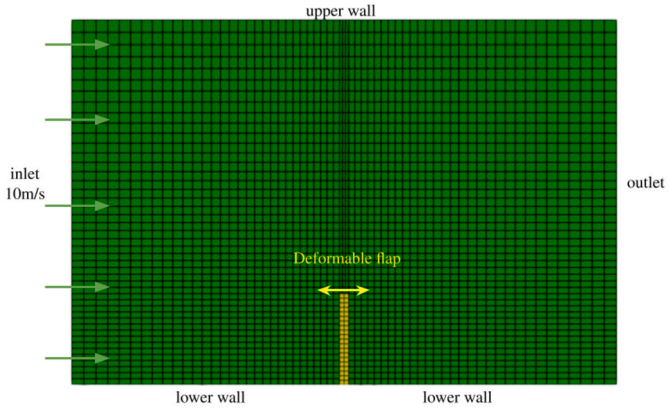

Fig. 8. Case setup and boundary conditions for fluid-structure interaction case.

To achieve the particle-structure interaction, only two data fields are needed. These data fields are exchanged over nodes of the FEM mesh. Fig. 7 (a) shows a FEM structure with its mesh along with the nodes that are used to share data. Hence, for this particular DEM-FEM coupling, it is crucial to have a mesh good enough to capture the particle impacts.

As described in section 2.1, equation (2.6), the $\vec{F}_i^c$ is the collision force between particles. In the XDEM software suite, the structure wall is treated just as another particle. This article uses an STL file to represent the geometry needed. The triangles are sub-shapes forming the particle. A binary tree search is done to find the exact triangle(s) where the collision takes place [61]. The particle impacts on these triangles are captured and interpolated onto the nodes. The force interpolation is based on the virtual work equivalent to ensure consistent nodal forces for the Finite Element Method (FEM). This approach allows the work of the particle force paired with the interpolated displacement to equal the work achieved by the nodal forces and nodal displacement, ensuring an accurate representation of the forces on the triangles [61]. A detailed description of the contact prediction and interpolation algorithm can be found in the literature [86,87,61].

As these forces are interpolated onto the nodes of the STL, they communicated with the FEM solver. The preCICE coupling library uses data mapping schemes to apply these point loads onto the nodes. The point loads coming from particles and the fluid are summed up when necessary, mainly depending on the coupling exchange time step. The FEM solver then solves for the displacements of the structure and communicates the displacements to the other participants in the partitioned coupling. XDEM then deforms (or rather translates) the STL in its domain as per the displacements applied. This moves the STL wall within the DEM domain, thus representing the structure movement.

4. Results

In the Methods 2 and Coupling 3 section, we established how the coupling between different single-physics black box solvers is achieved. Although one can model a 6−way CFD-DEM-FEM coupling at this point, the multi-physics partitioned model needs to be tested.

To establish that this 6−way coupled modeling is correct certain physical phenomena are tested individually. Hence, in the results section, we will first go through coupling between two software and test out the 2−way coupling. This study will ascertain if the 2−way coupled physics works properly. And finally, we study the 6−way coupling. This step-by-step study of the coupled model not only reveals its strengths but also pushes the model to its limitations.

For each type of coupling, a format is followed, where we start with a general description of the test case, the goals to be achieved with the given case, simulation setup including individual physics boundary conditions (BC) and coupling parameters, and finally we see the results for the given case.

In the literature [88], usually a coupling CFD-DEM coupling is considered 2−way coupling, and inter-particle momentum exchange is also considered as 2−way coupling between individual particles. Hence the case presented here is usually known as a 4−way coupling. But as the focus of the current work is the coupling of two different physics, we consider this type of case as a 2−way coupling.

4.1. 2-way CFD-FEM coupling case: flow through channel

The first test case provided by the preCICE team [81], is a pseudo 2D version of the FSI case from [89]. In this case, there is a flexible perpendicular flap in a channel. This case demonstrates Fluid-Structure Interaction (FSI). Furthermore, this setup is used to expand and add particle physics as well.

A pseudo two-dimensional fluid flow through a channel is modeled [81]. A deformable flap is placed in the center of this channel. The perpendicular flap deforms and oscillates due to the fluid flow.

4.1.1. Simulation setup

The fluid domain is 6 m long in the x-direction, and 4 m in the y-direction. The deformable flap is 1 m long in the y-direction, and 0.1 m thick in the x-direction. The fluid inlet is located on the left side as seen in Fig. 8, where the fluid enters the simulation domain at 10 m/s. The upper and lower sides as enclosed and treated as wall boundaries. The deformable flap is treated as a moving boundary. Finally, the outlet is on the right side of the simulation domain. As this is a pseudo two-dimensional fluid flow, the front and back are empty boundaries.

The fluid mesh consists of 3150 hexahedrons as seen in Fig. 8. As the CFD uses the finite volume method (FVM), it needs a volume, hence the z-direction consists of one cell of arbitrary length. The deformable flap is divided into 20 equidistant divisions in the y-direction, 2 division parts in the x-direction, and 1 division in the z-direction. The FEM model uses $C3D8$ element [55]. A Dirichlet boundary condition is applied on the nodes at the bottom restricting the displacements to zero using the `*BOUNDARY` card, whereas a Neumann boundary condition is applied on the rest of the nodes, where point forces are applied using the `*CLOAD` card.

The fluid density (ρ_f) is 1 kg/m^3, and the deformable flap density (ρ_s) is 3000 kg/m^3. The fluid kinematic viscosity $\nu_f = 1$ m/s^2. The deformable flap's Young's Modulus E $= 4 \times 10^6$ kg/ms^2, and the Poisson ration $\nu_s = 0.3$.

The CFD uses a time-step of 10^{-4} s, FEM uses a time-step of 10^{-2} s, whereas the coupling time-step between the CFD and FEM is set to 10^{-2} s. The `nearest-neighbor` mapping scheme is used for data mapping from CFD to FEM, whereas `nearest-projection` mapping scheme is used for data mapping from FEM to CFD.

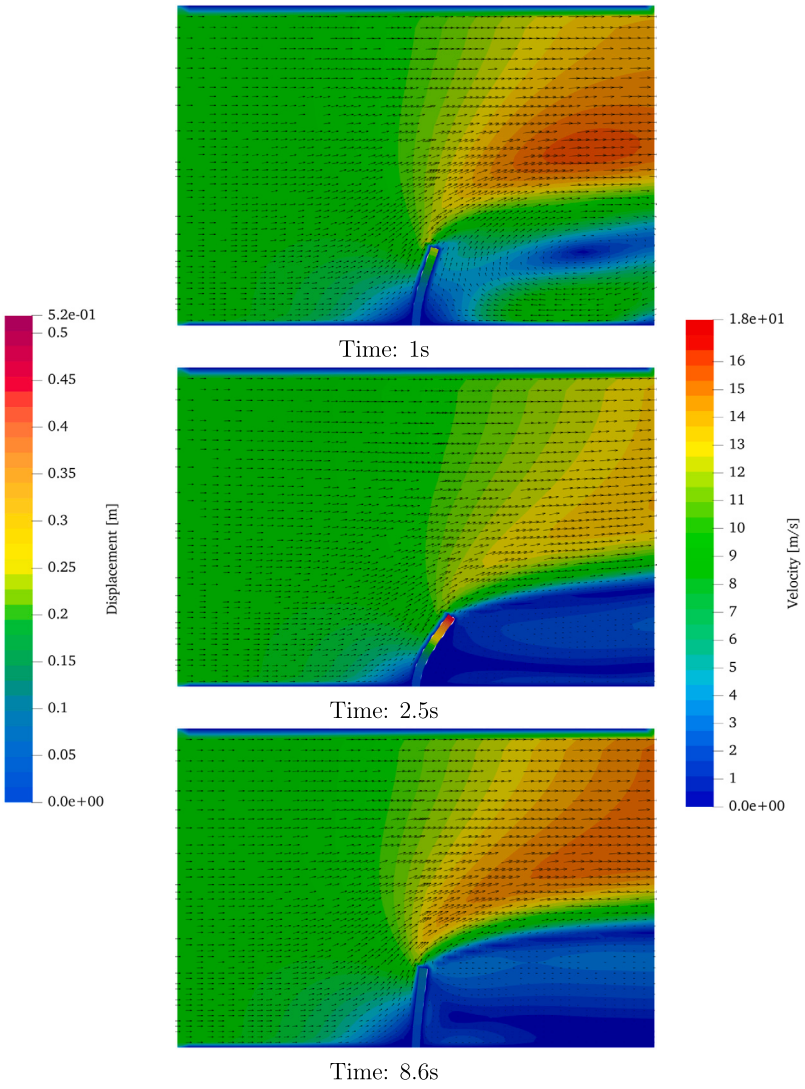

Fig. 9. Fluid flow through the channel deforming the perpendicular flap.

4.1.2. *Results for 2-way coupling case*

The flexible perpendicular flap moves because of the fluid flow acting on it. A point on the flap is monitored for displacements and this displacement is plotted over time, presented in Fig. 10. Additionally, the normalized forces acting at the tip in the x-direction are presented in Fig. 11. An oscillatory behavior in the displacement can be clearly seen in the 10 due to the pressure built up.

Fig. 9, a slice of 2D fluid field showing the fluid velocity as well as the deformable flap show displacements are presented for different instances in the simulation. The Fig. 10, and Fig. 11 can be used to cross-verify the fluid-structure interaction.

This section establishes the FSI, where fluid is the momentum source causing the displacements in the deformable flap.

4.2. *6-way CFD-DEM-FEM coupling case: flow through channel (pseudo 2D)*

In section 4.1, the FSI case with a fluid flow through the channel is established. In the current section, the same case is extended to include the effects of particles on the fluid flow as well as structure deformation. In this case, the fluid momentum is still the main driving force.

This case is considered to be pseudo 2D, as only the fluid domain is solved in two dimensions, i.e. we have only one cell in the width. On the contrary, the FEM and DEM domains are fully 3D. This is done to have the same case setup as the FSI presented in the previous section.

4.2.1. *Simulation setup*

The simulation setup for the fluid and the structure remains the same as described in section 4.1.1. The only change made to the structure solver is that the FEM solver time step is reduced from $10^{-}2$ s to $10^{-}4$ s. This change is made to capture the particle impacts with sufficient temporal resolution.

The DEM simulation time-step used is 10^{-5} s. This is much lower than the other two counterparts to allow detection of particle collisions. The Hertz-Mindlin collision model is used, as described in the section 2.1. The gravity is pointing in the negative z-direction, with $\vec{g} = 9.81$ m/s^2.

There are two types of particles, heavy and light injected into the simulation domain as shown in Fig. 12. The mechanical properties of these particles are given in the Table 1. These particles are used to demonstrate the different effects of fluid forces acting on the particles. The heavy particles are injected using a particle source located at $(-3, 0.15, 3.25)$ m. The particle source size is 0.05×0.25 m. The heavy particles are injected with an initial velocity of 1 m/s, with a particle rate of 50 particles/s, with a time-step of 10^{-5} s. The coupling time-step between the DEM and FEM is set to 10^{-3} s. The coupling time-step between the DEM and CFD is set to 10^{-3} s.

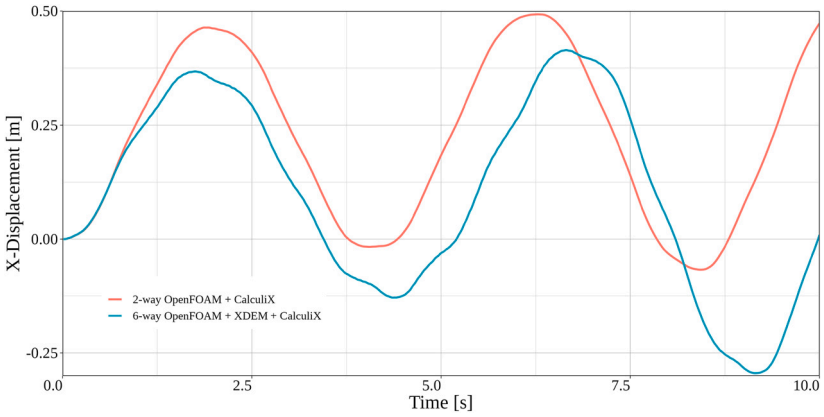

Fig. 10. Displacement of flap tip monitored over time caused due to FSI and FPSI.

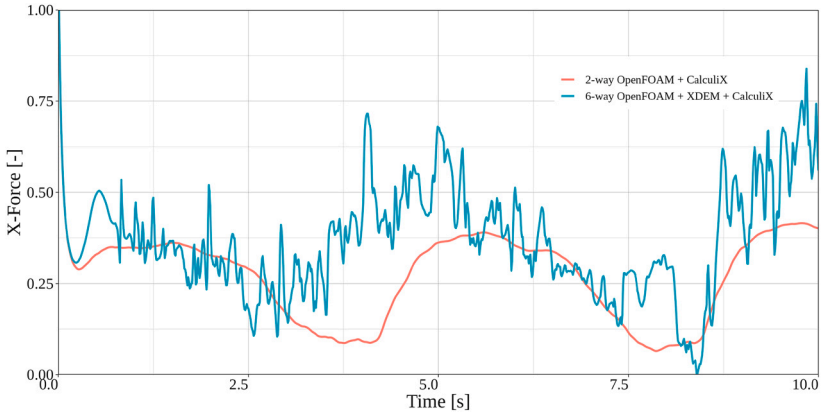

Fig. 11. Normalised x-direction forces acting on the deformable flap tip.

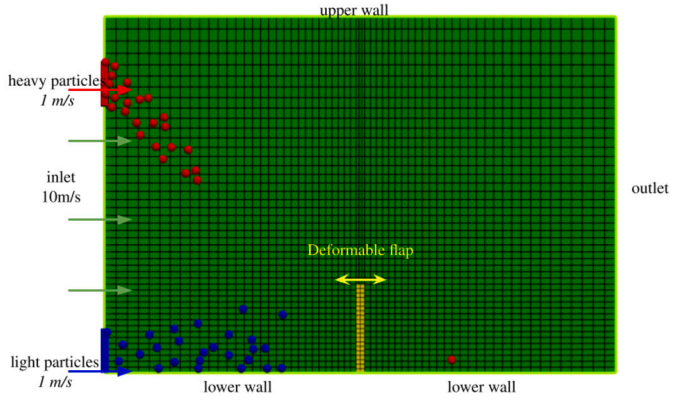

Fig. 12. Case setup and boundary conditions for fluid-structure interaction case.

Table 1
Physical and Mechanical properties of the particles used in the DEM model.

Properties	Heavy particles	Light Particles
Density ρ (kg/m^3)	50	0.5
Young's Modulus (Pa)	5×10^5	5×10^5
Poisson Ratio [-]	0.45	0.45
Spring Stiffness [N/m]	1×10^5	1×10^5
Coefficient of Restitution	0.5	0.5
Coefficient of Static Friction	0.8	0.8
Coefficient of rolling friction	0.15	0.15

4.2.2. Results for 6-way coupling case (pseudo 2D)

As seen in the previous section, the fluid is the main momentum source in this simulation as well. The fluid transfers momentum to the particles as well as the deformable flap. In the Fig. 13, both the heavy and light particles are transported in the direction of the fluid flow.

In the current example, there are two types of particles being used in the simulation domain, heavy and light. As the name suggests, they are either heavier or lighter than the fluid. This not only allows us to check for momentum transfer but also the buoyancy forces acting on the particles. The Fig. 13, shows temporal evolution, where the heavy particles are observed to be transported in the fluid flow direction, as well as sink in the fluid domain due to being heavier than the fluid. On the contrary, the lighter particles are seen to rise as they are being transported by the fluid. This demonstrates that the buoyancy forces are working correctly.

The fluid velocity field seen at time 1 s in Fig. 9 and Fig. 13 is similar, as the particles have yet to alter the fluid flow. The fluid velocity field in the Fig. 13, additionally shows the drag offered by the particles to the fluid flow. A consistent lower velocity is observed just at the particle injection points due to the consistent presence of the particles. As the simulation progresses, the particles start filling up the space left of the deformable flap. As opposed to the unrestricted fluid flow seen to the left side of the deformable flap in Fig. 9, due to the blockage caused by particles, the fluid flow is heavily restricted. Due to this particle blockage, the fluid flow is changed quite drastically for the 6−way FPSI coupled scenario as compared to the 2-way FSI case, especially observed in at time 8.6 s in Fig. 9 and Fig. 13 respectively.

The Fig. 10, further confirms this altered flow through the displacement of the deformable flap tip. The flap tip displacement for the FSI Case 4.1, is oscillatory in nature and has a consistent amplitude over

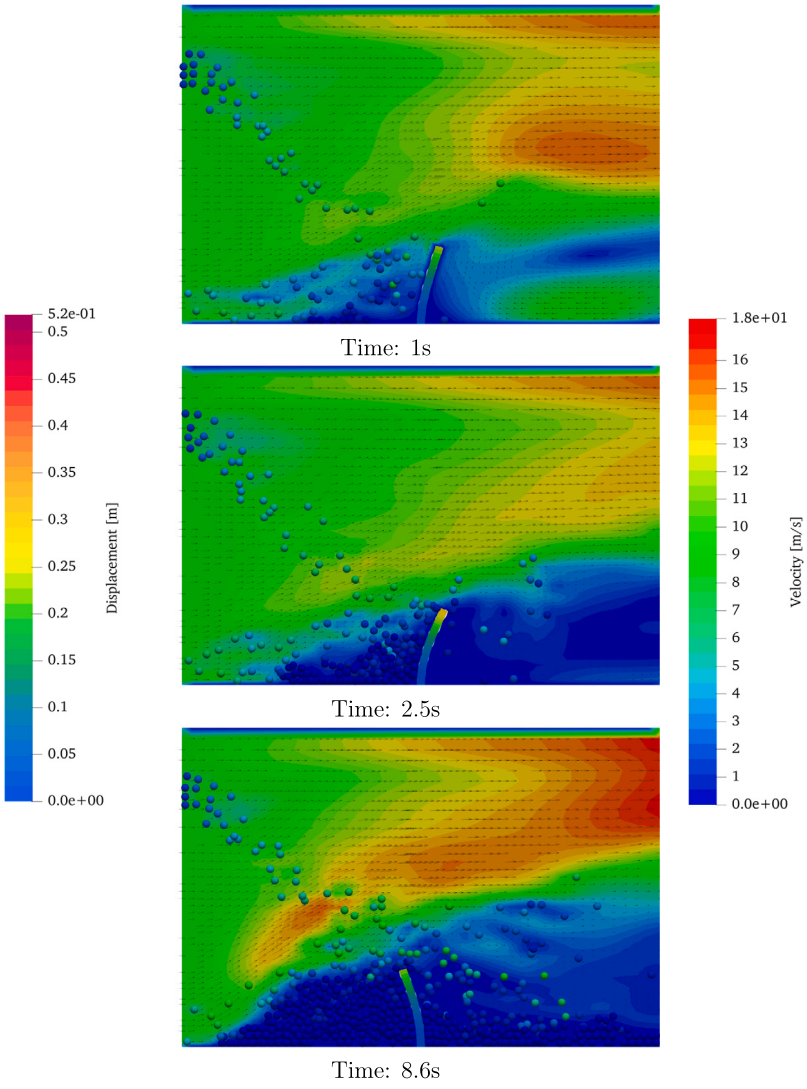

Fig. 13. Fluid flow through the channel deforming the perpendicular flap.

time. On the contrary, for the 6−way FPSI case, although some oscillatory behavior is seen for the flap tip displacement, it is clearly altered. The reason behind this altered behavior is further confirmed by Fig. 11, illustrating the x-direction forces acting at the flap tip. For the FSI case, as only fluid forces are acting on the flap represented in red, the forces are seen to act in an oscillatory manner, thus resulting in oscillatory displacements. On the contrary, the forces acting on the flap tip for the 6−way FPSI case, the forces are a lot more erratic in nature. This is because the forces acting on the flap included the fluid as well as the particle forces. Although these forces are very erratic, if a time-averaged force is plotted, it can be seen that there is still an oscillatory pattern. Additionally, due to the clumping of particles on the deformable flap, a higher overall force is acting on the flap leading to more deformation compared to 2−way case, as seen in Fig. 10.

4.3. Flow through channel: insights into 3D results

In this section, the cases are presented in the modified 3 dimensional format. This is to demonstrate that the proposed coupling approach works not only for 2 dimensions (2D) but also for 3 dimensions (3D). The cases presented above were built on from the literature, hence they are pseudo 2D in nature, where the fluid is solved as a 2D case, whereas functionally, the FEM and DEM participants are 3D, and solved accordingly.

In the current section, we consider the same cases as presented in the previous section 4.1 and 4.2, however, the fluid domain has 5 cells in the z-axis with a length of 0.3 m thickness, making it a truly 3D problem. The solid flap is also discretized in the z-direction into 5 cells with 0.3 m thickness. With the discretization in the z-direction, the results presented in the current section are pure 3D.

All the simulation set-up remains the same as mentioned in section 4.1 and 4.2, except that a no-slip boundary condition is applied on the walls instead of the `empty` boundary condition. The Fig. 14 shows the new discretization of the solid and the triangulated mesh used to represent the structure in the XDEM domain. The figure also shows the nodes used to exchange data to and from the structure solver.

In the Fig. 15, a 3D snapshot of the particle-laden flow through the channel is shown. The arrows show the fluid velocity direction and magnitude. The perpendicular flap shows uniform displacements in the z-direction. The particles can be seen to be obstructed by the perpendicular flap.

The Fig. 16 compares the displacement for the different cases presented. As the flow through channel case is extended to 3D, the displacement is qualitatively similar to that seen in the pseudo 2D cases. The 2-way CFD-FEM case is also extended to be 3D, where the displacements are seen to be slightly different than seen in section 4.1.

For the 6-way CFD-DEM-FEM case, as the domain is extended in the third direction, the fluid can exert forces more evenly across the perpen-

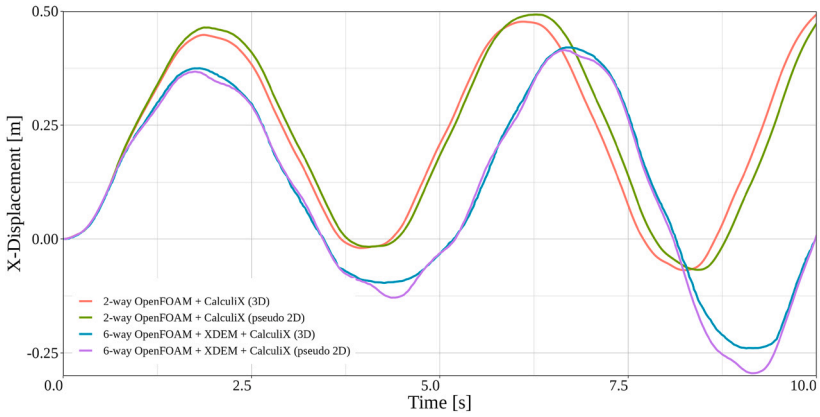

Fig. 16. Comparison of the perpendicular flap tip displacement for (pseudo)2D and 3D cases.

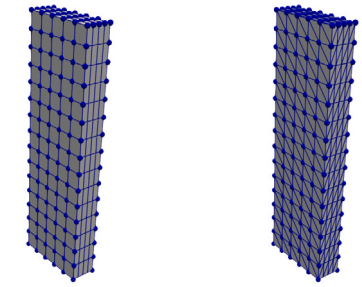

(a) FEM mesh with nodes (b) XDEM STL wall with nodes

Fig. 14. FEM and XDEM wall mesh with the nodes used to exchange data with fives cells in z-direction.

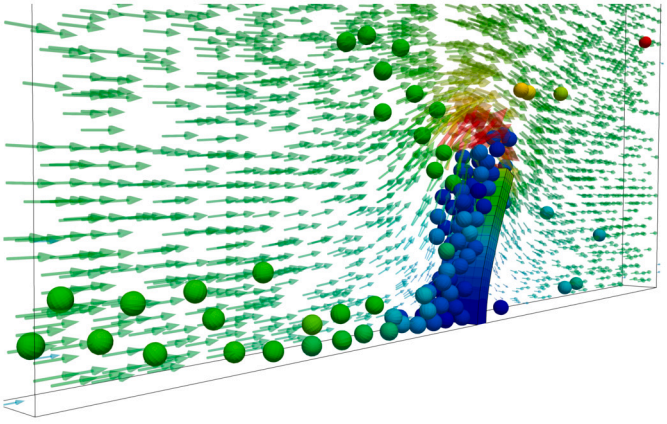

Fig. 15. A 3D snapshot of the simulation at 2.5 s for the 6-way CFD-DEM-FEM coupling.

dicular flap, muting the erratic displacements seen in pseudo 2D case, giving rise to more stable displacement oscillations. However, the overall forces exerted by the presence of particles and the alteration of the fluid flow keep the displacement for 3D case closer to those observed in the pseudo 2D case.

4.4. 6-way CFD-DEM-FEM coupling case: particle flow

In the section 4.2, a 6−way CFD-DEM-FEM momentum coupling was presented, where fluid flow is the driving force. Conversely, in the current section, the fluid is stand-still, and the particles are injected in the simulation domain at high velocity. The particle induces momentum on fluid, that indirectly moves the perpendicular flap.

4.4.1. Simulation setup

The simulation setup is similar as described in section 4.2.1. The only change to the fluid simulation setup is, that the inlet velocity is set to zero. The light particles are not injected, while the heavy particles are injected at 10 m/s.

4.4.2. Results for 6-way coupling case: particle flow

The Fig. 18, illustrates the temporal evolution of the fluid velocity field as the particles are injected in the simulation domain. As the particles are injected and the fluid is at a standstill, the semi-implicit momentum source term is injected (as described in equation (2.19)), and a fluid flow is established. The momentum exchange and the fluid drag forces exerted on the particles make them lose their initial velocity, thus dropping to the bottom as they are about to reach the right extreme of the simulation domain.

The fluid velocity in the section 4.1 and section 4.2, was 10 m/s. In the current numerical experiment, although the particles have an initial velocity of 10 m/s, the fluid does not move at the same velocity. Additionally, only the fluid directly in the path of particles is affected the most, whereas the rest of the flow is established due to indirect interactions. Due to these factors, the deformable flap does not move as much as seen in Fig. 17. This numerical experiment established the direct and indirect momentum exchange between the particles, fluid and, structure.

5. Discussion

The partitioned coupling approach presents a lot of benefits and flexibility as compared to the monolithic coupling approach. The literature contains a lot of work done to enable partitioned coupling approach through the use of external libraries [48,42,44–47]. Although, these are applied to or restricted to only certain types of applications. In the context of fluid-particle-structure interaction, the literature is sparse, and it is even more so when considering the partitioned coupling approach used for FPSI.

The section 3, an in-depth description of the partitioned coupling approach is presented. This section delves into the development process of the preCICE adapters for single physics solvers. The mathematical formulations to consider the effects of different physics are presented thoroughly in the section 2.4 and section 2.5. Thus the authors believe that the current work provides a complete concept and notion of achieving a 6-way CFD-DEM-FEM momentum coupling via a partitioned coupling approach. This approach allows for the exchange/swap of any of the single physics solvers involved thus allowing engineers and researchers to easily couple a single physics solver/software to achieve FPSI.

The results section 4, presents numerical experiments involving a preliminary 2−way CFD-FEM coupling (FSI). This case successfully

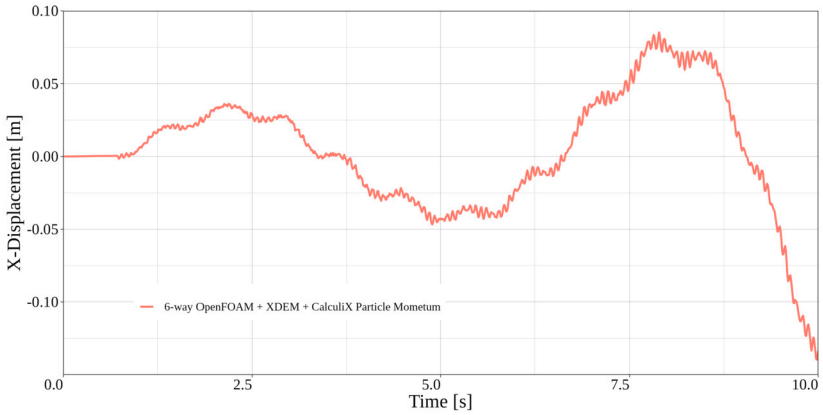

Fig. 17. Displacement of flap tip caused due to indirect interaction with the particle flow.

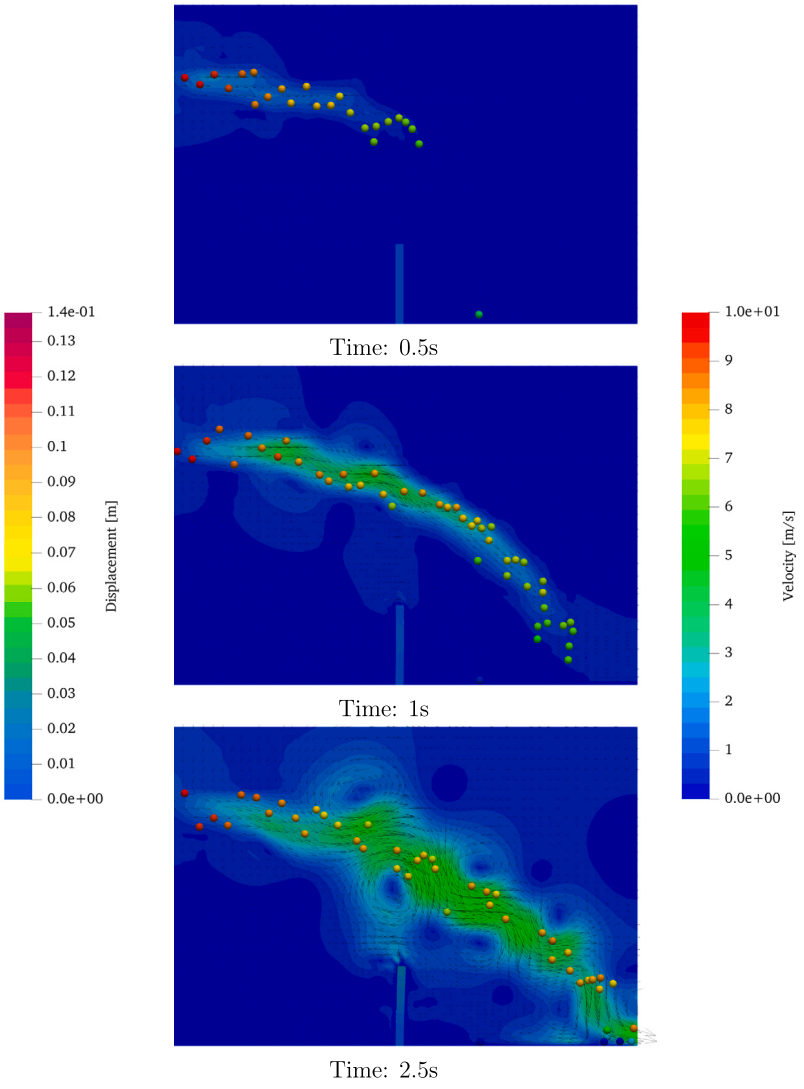

Fig. 18. Fluid flow through the channel deforming the perpendicular flap.

demonstrates the fluid-structure interaction, with additional FSI validation available in literature [50]. This case demonstrates the oscillatory displacement of the perpendicular flap tip due to the influence of fluid flow. The fluid forces acting on the tip further support this displacement pattern.

This 2−way CFD-FEM coupling is expanded to include particle physics, thus turning it into 6−way CFD-DEM-FEM coupling. In the section 4.2, the fluid remains the primary source of momentum. This momentum is successfully transferred to particles along with the flap. The different density particles also demonstrate the fluid buoyancy acting on the particles. The deformable flap is affected by both fluid and particle forces acting on it, demonstrated by the forces acting on the tip. Furthermore, the flap tip displaces in an oscillatory manner, similar to that in the 2−way CFD-FEM case, but the displacement amplitudes and

temporal evolution are heavily influenced due to the presence of particles. On the contrary, in the section 4.4, particles indirectly displace the perpendicular flap, still displaying an oscillatory displacement pattern, but with much lower amplitude due to the lower fluid velocities. This case also successfully demonstrates the bi-directional nature of the coupling between the different single physics solvers.

The current CFD-DEM coupling established is of an un-resolved type, hence only a global interaction can be achieved. The intricate particle-fluid interaction cannot be resolved with the unresolved coupling. Although, this is a limitation of the unresolved CFD-DEM coupling rather than the partitioned coupling approach. Another caution when using this coupling is to have FEM and STL resolved enough to capture the particle impacts correctly. This is because the particle impact is captured on the triangular sub-shape of the STL file representing the structure in the DEM domain. These forces are distributed on the three nodes of the triangle, that are applied as point loads on the FEM mesh. If these triangles are too big, the forces might be applied too far from the actual point of impact thus leading to erroneous behavior. Similarly, when representing the structure deformations in the DEM domain, the STL nodes are "displaced" according to the displacements computed by FEM. If the STL mesh is not fine enough to represent the deformations computed by the FEM mesh, this might lead to the structure deformations represented incorrectly in the DEM domain.

This coupling is developed to solve real-world problems, such as erosion predictions and erosion monitoring inside the abrasive water jet cutting nozzle [90,91] that is currently being developed. The results presented in the current work only consider single-phase fluid, whereas a multi-phase fluid is being considered and developed as described in [90,91]. Additionally, the partitioned CFD-DEM coupling approach has been developed [92] and applied to steel-making processes such as Midrex blast furnace [41].

There are many more engineering applications, that involve fluid, structure, and particle interactions. But often one of the interactions, or even worse one of the physics is entirely ignored to reduce complexity. The partitioned coupling approach presented in the current work is very flexible and can be used or extended to involve even more physics.

6. Conclusion

In conclusion, this work introduces a comprehensive and novel approach to achieve a 6−way CFD-DEM-FEM momentum exchange using the partitioned coupling approach. This method is important because it is flexible enough to allow researchers and engineers to couple different single physics solvers for fluid, particle, and structure interactions interchangeably.

The developed preCICE adapters facilitate the coupling of single physics solvers, enabling a seamless momentum exchange between different single physics solvers to achieve fluid-particle-structure interactions (FPSI). The successful fluid-particle-structure interactions are demonstrated via numerical experiments. The foundation for a strong and adaptable coupling framework is laid by the mathematical formulations shown in the coupling equations, which demonstrate the methodical consideration of various physics.

Through sequential testing, the numerical experiments demonstrate the partitioned coupling approach. Fluid-structure interactions (FSI) are successfully captured by the first 2−way CFD-FEM coupling, which has been verified against previous research. Particle dynamics are introduced by extending this coupling to a 6−way CFD-DEM-FEM scenario, illustrating the intricate interaction between fluid, particles, and deformable structures.

In conclusion, the developed 6-way CFD-DEM-FEM momentum coupling, facilitated by a partitioned coupling approach, provides a flexible framework with wide-ranging applications across various engineering domains in addition to aiding in the understanding of FPSI. The successes and insights that have been demonstrated open up new avenues for the study of complex coupled physics phenomena.

Nomenclature

	Physical constants/Greek symbols
β	Interphase momentum exchange (kg/(m^3 s))
ϵ	Porosity
μ_f	Dynamic viscosity (Pa s)
μ	Sliding friction (-)
μ_r	Rolling Friction (-)
η	Weight of particle for porosity calculation
Ω_c	Implicitly treated drag term (1/s)
ρ	Density (kg/m^3)
	Operators
∂	Differential operator (-)
Δ	Difference (-)
∇	Nabla operator (-)
	Scalars
A	Surface Area
C_d	Drag Coefficient (-)
d	Particle diameter (m)
I_i	Moment of inertia (kg m^2)
m	Mass (kg)
p	Pressure (Pa)
r, R	Radius (m)
Re	Reynolds number (-)
t	Time (s)
T_{final}	Length of simulation (s)
V	Volume (m^3)

	Subscripts
c	Cell, collision
d	Drag
eff	Effective values
f	Fluid
g	Gravity
i, j	Particle
n	Normal direction
p, P	Particle
s	Solid
t	Tangential direction
	Superscripts
n	Geometry exponent
(n)	n^{th} (time) step
$(n+1)$	n^{th} (time) step +1
	First order tensors (vectors)
$\vec{A}_c$	Acceleration on fluid cell due to explicitly treated drag term (m/s^2)
$\vec{g}$	Gravitational acceleration (m/s)
$\vec{F}^c$	Contact Forces (N)
$\vec{F}^g$	Gravitational Force (N)
$\vec{F}^{ext}$	External Forces (N)
$\vec{F}_B$	Buoyancy Force (N)
$\vec{F}_D$	Drag Force (N)
$\vec{M}$	Torque (N m)
$\vec{v}$	Velocity
$\vec{X}_i$	Positional vector (m)
$\vec{\omega}$	Rotational velocity (rad/s)
$\vec{\phi}$	Orientation (deg)

CRediT authorship contribution statement

Prasad Adhav: Writing – review & editing, Writing – original draft, Visualization, Validation, Software, Methodology, Investigation, Formal analysis, Data curation, Conceptualization. **Xavier Besseron:** Writing – review & editing, Validation, Supervision, Software, Methodology, Formal analysis. **Bernhard Peters:** Supervision, Resources, Project administration, Investigation, Funding acquisition, Formal analysis, Conceptualization.

Declaration of competing interest

The authors declare that they have no known competing financial interests or personal relationships that could have appeared to influence the work reported in this paper.

Data availability

Data will be made available on request.

Acknowledgement

This research was partially supported by Luxembourg National Research Fund (project numbers 13558062 and 14843353).

References

[1] Gene Hou, Jin Wang, Anita Layton, Numerical methods for fluid-structure interaction—a review, Commun. Comput. Phys. 12 (2) (2012) 337–377.
[2] Woojin Kim, Haecheon Choi, Immersed boundary methods for fluid-structure interaction: a review, Int. J. Heat Fluid Flow 75 (2019) 301–309.
[3] Eugenio Oñate, et al., The particle finite element method—an overview, Int. J. Comput. Methods 1 (02) (2004) 267–307.
[4] Moubin Liu, Zhilang Zhang, Smoothed particle hydrodynamics (SPH) for modeling fluid-structure interactions, Sci. China, Phys. Mech. Astron. 62 (2019) 1–38.
[5] Fei Xu, et al., On methodology and application of smoothed particle hydrodynamics in fluid, solid and biomechanics, Acta Mech. Sin. 39 (2) (2023) 722185.
[6] Ramji Kamakoti, Wei Shyy, Fluid–structure interaction for aeroelastic applications, Prog. Aerosp. Sci. 40 (8) (2004) 535–558.
[7] Syed Samar Abbas, Mohammad Shakir Nasif, Rafat Al-Waked, State-of-the-art numerical fluid–structure interaction methods for aortic and mitral heart valves simulations: a review, Simulation 98 (1) (2022) 3–34.
[8] Yuri Bazilevs, et al., Computer modeling of wind turbines: 2. free-surface FSI and fatigue-damage, Arch. Comput. Methods Eng. 26 (2019) 1101–1115.
[9] Siddharth Suhas Kulkarni, et al., Fluid-structure interaction based optimisation in tidal turbines: a perspective review, J. Ocean Eng. Sci. 7 (5) (2022) 449–461.
[10] Tajammal Abbas, Igor Kavrakov, Guido Morgenthal, Methods for flutter stability analysis of long-span bridges: a review, in: Proceedings of the Institution of Civil Engineers, Bridge Eng. 170 (4) (2017) 271–310, Thomas Telford Ltd.
[11] A.S. Tijsseling, Fluid-structure interaction in liquid-filled pipe systems: a review, J. Fluids Struct. 10 (2) (1996) 109–146.
[12] Vincent Keim, et al., FSI-simulation of ductile fracture propagation and arrest in pipelines: comparison with existing data of full-scale burst tests, Int. J. Press. Vessels Piping 182 (2020) 104067.
[13] Bernhard Peters, et al., XDEM multi-physics and multi-scale simulation technology: review of DEM–CFD coupling, methodology and engineering applications, Particuology 44 (2019) 176–193.
[14] Xiaoyu Wang, et al., Developments and applications of the CFD-DEM method in particle–fluid numerical simulation in petroleum engineering: a review, Appl. Therm. Eng. 222 (2023) 119865.
[15] Shibo Kuang, Mengmeng Zhou, Aibing Yu, CFD-DEM modelling and simulation of pneumatic conveying: a review, Powder Technol. 365 (2020) 186–207.
[16] Navid Aminnia, et al., Three-dimensional CFD-DEM simulation of raceway transport phenomena in a blast furnace, Fuel 334 (2023) 126574.
[17] Mahmoud A. El-Emam, et al., Theories and applications of CFD–DEM coupling approach for granular flow: a review, Arch. Comput. Methods Eng. (2021) 1–42.
[18] Zhenjiang Zhao, et al., Recent advances and perspectives of CFD–DEM simulation in fluidized bed, Arch. Comput. Methods Eng. (2023) 1–48.
[19] Prasad Adhav, et al., Numerical insights into rock–ice avalanche geophysical flow mobility through CFD–DEM simulation, Comput. Part. Mech. (2024), https://doi.org/10.1007/s40571-023-00699-3.
[20] Fanbao Chen, et al., Sand-ejecting fire extinguisher parameter sensitivity analysis based on DOE and CFD-DEM coupling simulations, Adv. Powder Technol. 33 (9) (2022) 103719.
[21] Yong Kong, Jidong Zhao, Xingyue Li, Hydrodynamic dead zone in multiphase geophysical flows impacting a rigid obstacle, Powder Technol. 386 (2021) 335–349.
[22] Liming Yao, et al., An optimized CFD-DEM method for particle collision and retention analysis of two-phase flow in a reduced-diameter pipe, Powder Technol. 405 (2022) 117547.
[23] Dan Forsström, Pär Jonsén, Calibration and validation of a large scale abrasive wear model by coupling DEM-FEM: local failure prediction from abrasive wear of tipper bodies during unloading of granular material, Eng. Fail. Anal. 66 (2016) 274–283.
[24] Yogesh Surkutwar, Corina Sandu, Costin Untaroiu, Review of modeling methods of compressed snow-tire interaction, J. Terramech. 105 (2023) 27–40.
[25] Boqiang Wu, et al., Numerical simulation of erosion and fatigue failure the coal gangue paste filling caused to pumping pipes, Eng. Fail. Anal. 134 (2022) 106081.
[26] Wei Wang, et al., Using FEM–DEM coupling method to study three-body friction behavior, Wear 318 (1–2) (2014) 114–123.
[27] Seddik Shiri, 3D numerical modeling of flows on a reduced model of a ski jump spillway with an erosion pit using a coupled SPH–FEM-DEM approach, J. Appl. Water Eng. Res. (2023) 1–13.
[28] Alessandro Leonardi, et al., Particle–fluid–structure interaction for debris flow impact on flexible barriers, Comput.-Aided Civ. Infrastruct. Eng. 31 (5) (2016) 323–333.
[29] Chun Liu, Zhixiang Yu, Shichun Zhao, A coupled SPH-DEM-FEM model for fluid-particle-structure interaction and a case study of Wenjia gully debris flow impact estimation, Landslides 18 (2021) 2403–2425.
[30] L.M. Yao, et al., A new multi-field coupled dynamic analysis method for fracturing pipes, J. Pet. Sci. Eng. 196 (2021) 108023.
[31] Davood Beyralvand, Farzad Banazadeh, Rasoul Moghaddas, Numerical investigation of novel geometric solutions for erosion problem of standard elbows in gas-solid flow using CFD-DEM, Results Eng. 17 (2023) 101014.
[32] Samanthi Indiketiya, Piratheepan Jegatheesan, Pathmanathan Rajeev, Evaluation of defective sewer pipe–induced internal erosion and associated ground deformation using laboratory model test, Can. Geotech. J. 54 (8) (2017) 1184–1195.
[33] R. Parameshwaran, Sai Jathin Dhulipalla, Daseswara Rao Yendluri, Fluid-structure interactions and flow induced vibrations: a review, Proc. Eng. 144 (2016) 1286–1293.
[34] Pär Jonsén, et al., A novel method for modelling of interactions between pulp, charge and mill structure in tumbling Mills, Miner. Eng. 63 (2014) 65–72.
[35] Simon Larsson, et al., A novel approach for modelling of physical interactions between slurry, grinding media and mill structure in wet stirred media Mills, Miner. Eng. 148 (2020) 106180.
[36] Dong-Mei Zhang, Lei Han, Zhong-Kai Huang, A numerical approach for fluid-particle-structure interactions problem with CFD-DEM-CSD coupling method, Comput. Geotech. 152 (2022) 105007.
[37] Gabriele Pozzetti, et al., A co-located partitions strategy for parallel CFD–DEM couplings, Adv. Powder Technol. 29 (12) (2018) 3220–3232.
[38] Sergio R. Idelsohn, Numerical Simulations of Coupled Problems in Engineering, Springer, 2014.
[39] Benjamin Walter Uekermann, Partitioned fluid-structure interaction on massively parallel systems, PhD thesis, Technische Universität München, 2016.
[40] Xavier Besseron, Henrik Rusche, Bernhard Peters, Parallel multi-physics simulation of biomass furnace and cloud-based workflow for SMEs (English), in: Practice and Experience in Advanced Research Computing (PEARC '22), CE - Commission Européenne [BE], Association for Computing Machinery, Boston, MA, United States, July 2022, https://pearc.acm.org/pearc22/pearc.acm.org/pearc22/.
[41] Xavier Besseron, Prasad Adhav, Bernhard Peters, Parallel multi-physics coupled simulation of a midrex blast furnace, in: Proceedings of the HPC Asia 2024 Workshops, Association for Computing Machinery, New York, NY, United States, 2024.
[42] Florent Duchaine, et al., Analysis of high performance conjugate heat transfer with the openpalm coupler, Comput. Sci. Discov. 8 (1) (2015) 015003.
[43] S. Slattery, P.P.H. Wilson, R. Pawlowski, The Data Transfer Kit: a geometric rendezvous-based tool for multiphysics data transfer, in: International Conference on Mathematics & Computational Methods Applied to Nuclear Science & Engineering (M&C 2013), 2013, pp. 5–9.
[44] F.I. Pelupessy, et al., The astrophysical multipurpose software environment, Astron. Astrophys. 557 (2013) A84.
[45] Francesco Di Natale, et al., A massively parallel infrastructure for adaptive multiscale simulations: modeling RAS initiation pathway for cancer, in: Proceedings of the International Conference for High Performance Computing, Networking, Storage and Analysis, 2019, pp. 1–16.
[46] V.V. Krzhizhanovskaya, et al., Preface: Twenty Years of Computational Science, Lecture Notes in Computer Science, vol. 12142, 2020.
[47] Yu-Hang Tang, et al., Multiscale universal interface: a concurrent framework for coupling heterogeneous solvers, J. Comput. Methods Phys. 297 (2015) 13–31.
[48] Gerasimos Chourdakis, et al., preCICE v2: a sustainable and user-friendly coupling library, Open Res. Eur. 2 (2022).
[49] Derek Groen, et al., Mastering the scales: a survey on the benefits of multiscale computing software, Philos. Trans. R. Soc. A 377 (2142) (2019) 20180147.
[50] Gerasimos Chourdakis, David Schneider, Benjamin Uekermann, OpenFOAM-preCICE: coupling OpenFOAM with external solvers for multi-physics simulations, OpenFOAM® J. 3 (2023) 1–25.

[51] Benjamin Uekermann, et al., Official preCICE adapters for standard open-source solvers, in: Proceedings of the 7th GACM Colloquium on Computational Mechanics for Young Scientists from Academia, 2017.
[52] Lucia Cheung Yau, Conjugate Heat Transfer with the Multiphysics Coupling Library preCICE, Master's thesis, Technical University of Munich, 2016.
[53] OpenFOAM Foundation https://openfoam.org (first accessed: 2020).
[54] Guido Dhondt, The Finite Element Method for Three-Dimensional Thermomechanical Applications, John Wiley & Sons, 2004.
[55] Calculix – a free software three-dimensional structural finite element program, http://www.calculix.de/ (first accessed: 2020).
[56] Mehdi Baniasadi, Maryam Baniasadi, Bernhard Peters, Coupled CFD-DEM with heat and mass transfer to investigate the melting of a granular packed bed, Chem. Eng. Sci. 178 (2018) 136–145.
[57] Heinrich Hertz, Ueber die Berührung fester elastischer Körper, 1882.
[58] Raymond David Mindlin, Compliance of elastic bodies in contact, 1949.
[59] Yutaka Tsuji, Toshitsugu Tanaka, T. Ishida, Lagrangian numerical simulation of plug flow of cohesionless particles in a horizontal pipe, Powder Technol. 71 (3) (1992) 239–250.
[60] D. Zhang, W.J. Whiten, The calculation of contact forces between particles using spring and damping models, Powder Technol. 88 (1) (1996) 59–64.
[61] Mark Michael, Frank Vogel, Bernhard Peters, DEM–FEM coupling simulations of the interactions between a tire tread and granular terrain, Comput. Methods Appl. Mech. Eng. 289 (2015) 227–248.
[62] Peter A. Cundall, Otto D.L. Strack, A discrete numerical model for granular assemblies, Geotechnique 29 (1) (1979) 47–65.
[63] Olek C. Zienkiewicz, Robert L. Taylor, Jian Z. Zhu, The Finite Element Method: Its Basis and Fundamentals, Elsevier, 2005.
[64] Olek C. Zienkiewicz, Robert L. Taylor, The Finite Element Method for Solid and Structural Mechanics, Elsevier, 2005.
[65] Gerhard A. Holzapfel, Nonlinear solid mechanics: a continuum approach for engineering science, 2002.
[66] Klaus-Jürgen Bathe, Finite element procedures, 2006, Klaus-Jurgen Bathe.
[67] Tao Zhao, Coupled DEM-CFD Analyses of Landslide-Induced Debris Flows, Springer, 2017.
[68] Links Schiller, A drag coefficient correlation, Z. Ver. Dtsch. Ing. 77 (1933) 318–320.
[69] Wei Du, et al., Computational fluid dynamics (CFD) modeling of spouted bed: assessment of drag coefficient correlations, Chem. Eng. Sci. 61 (5) (2006) 1401–1420.
[70] J.F.T. Richardson, Sedimentation and fluidization: part-1, Trans. Inst. Chem. Eng. 32 (1954) 35–53.
[71] Dimitri Gidaspow, Multiphase Flow and Fluidization: Continuum and Kinetic Theory Descriptions, Academic Press, 1994.
[72] Sabri Ergun, Ao Ao Orning, Fluid flow through randomly packed columns and fluidized beds, Ind. Eng. Chem. 41 (6) (1949) 1179–1184.
[73] C.Y. Wen, Y.H. Yu, Mechanics of fluidization, Chem. Eng. Prog. Symp. Ser. 162 (1966) 100–111.
[74] Renzo Di Felice, Marco Rotondi, Fluid-particle drag force in binary-solid suspensions, Int. J. Chem. React. Eng. 10 (1) (2012).
[75] Madhava Syamlal, William Rogers, Thomas J. OBrien, MFIX documentation theory guide, Tech. Rep., USDOE Morgantown Energy Technology Center (METC), WV (United States), 1993.
[76] Jin Sun, Francine Battaglia, Shankar Subramaniam, Hybrid two-fluid DEM simulation of gas-solid fluidized beds, 2007.
[77] Hamid Arastoopour, Numerical simulation and experimental analysis of gas/solid flow systems: 1999 Fluor-Daniel plenary lecture, Powder Technol. 119 (2–3) (2001) 59–67.
[78] Heng Xiao, Jin Sun, Algorithms in a robust hybrid CFD-DEM solver for particle-laden flows, Commun. Comput. Phys. 9 (2) (2011) 297–323.
[79] Isaak E. Idelchik, Handbook of Hydraulic Resistance, 1986, Washington.
[80] R.B. Bird, W.E. Stewart, E.N. Lightfoot, Transport Phenomena, 2nd edn, John Wilwe & Sons, New York, NY, 2007.
[81] preCICE Coupling Library official page www.precice.org (first accessed: 2020).
[82] A.W. Mainassara Chekaraou, et al., Hybrid MPI+OpenMP implementation of eXtended discrete element method, in: 2018 30th International Symposium on Computer Architecture and High Performance Computing (SBAC-PAD), Sept. 2018, pp. 450–457.
[83] Xavier Besseron, et al., Toward high-performance multi-physics coupled simulations for the industry with XDEM, in: 1st Conference Math 2 Product (M2P) on Emerging Technologies in Computational Science for Industry, Sustainability and Innovation, 2023.
[84] Gerasimos Chourdakis, A general OpenFOAM adapter for the coupling library preCICE, MA thesis, Technical University of Munich, Oct. 2017, https://www5.in.tum.de/pub/Chourdakis2017_Thesis.pdf.
[85] Stefan Turek, Jaroslav Hron, Proposal for Numerical Benchmarking of Fluid-Structure Interaction Between an Elastic Object and Laminar Incompressible Flow, Springer, 2006.
[86] H. Nakashima, A. Oida, Algorithm and implementation of soil–tire contact analysis code based on dynamic FE–DE method, J. Terramech. 41 (2–3) (2004) 127–137.
[87] David A. Horner, John F. Peters, Alex Carrillo, Large scale discrete element modeling of vehicle-soil interaction, J. Eng. Mech. 127 (10) (2001) 1027–1032.
[88] Shahab Golshan, et al., Review and implementation of CFD-DEM applied to chemical process systems, Chem. Eng. Sci. 221 (2020) 115646.
[89] Benedikt Schott, Christoph Ager, Wolfgang A. Wall, Monolithic cut finite element–based approaches for fluid-structure interaction, Int. J. Numer. Methods Eng. 119 (8) (2019) 757–796.
[90] Prasad Adhav, et al., AWJC nozzle simulation by 6-way coupling of DEM+ CFD+ FEM using preCICE coupling library, 2021.
[91] Prasad Adhav, Investigation of OpenFOAM-XDEM momentum coupling results for AWJC Nozzle using preCICE, 2023.
[92] Prasad Adhav, et al., Development and Validation of Cfd-Dem Coupling Interface for Heat & Mass Transfer Using Partitioned Coupling Approach, Available at SSRN 4668107, 2023.